Chapter 4

Effects of Amyloid-β Deposition on Mitochondrial Complex I Activity in Brain: A PET Study in Monkeys

Hideo Tsukada

Additional information is available at the end of the chapter

http://dx.doi.org/10.5772/62901

Abstract

This chapter discusses the capabilities of positron emission tomography (PET) imaging for the diagnosis of Alzheimer's disease (AD) with deposition of amyloid-β (Aβ). We conducted a PET scan using ^{18}F-2-tert-butyl-4-chloro-5-{6-[2-(2-fluoroethoxy)-ethoxy]-pyridin-3-ylmethoxy}-2H-pyridazin-3-one (^{18}F-BCPP-EF), a novel PET probe for mitochondrial complex I (MC-I) activity, in young and aged monkeys to demonstrate the normal aging effects on MC-I activity in the brain. The results revealed an age-related impairment of MC-I activity in the brain. Then, we conducted PET scan using ^{11}C-PIB to detect the Aβ deposition in the some parts, not all, of the brains of some part of aged monkeys. For further assessments, PET scans using ^{11}C-PIB for Aβ, ^{11}C-DPA-713 for inflammation, ^{18}F-fluoro-2-deoxy-D-glucose (^{18}F-FDG) for regional cerebral metabolic rate of glucose (rCMRglc), and ^{18}F-BCPP-EF for MC-I were performed in aged animals. When ^{18}F-BCPP-EF uptake is plotted against ^{11}C-PIB uptake in the cerebral cortical regions, it showed a significant negative correlation between them. Plotting of ^{11}C-DPA-713 uptake against ^{11}C-PIB resulted in a significant positive correlation. In contrast, plotting of rCMRglc against ^{11}C-PIB did not reach a statistically significant level. Taken together, these results strongly suggested that ^{18}F-BCPP-EF could discriminate the neuronally damaged areas with neuroinflammation where ^{18}F-FDG could not, owing to its high uptake into the activated microglia.

Keywords: Alzheimer's disease, aging, brain, mitochondrial complex I, PET

1. Introduction

Alzheimer's disease (AD) is neuropathologically characterized by the presence of neurofibrillary tangles with the deposition of hyperphosphorylated tau protein inside nerve cells and

senile plaques with extracellular aggregation of amyloid-β (Aβ) protein, and the imaging of tau and Aβ is expected to provide quantitative information noninvasively for the diagnosis of AD. Pathological aging processes are thought to be a degenerative process caused by accumulated damages, which leads to cellular dysfunction, tissue failure, and death, resulting in detectable changes in brain structure and function. Modern *in vivo* imaging techniques, such as X-ray computed tomography (X-CT), magnetic resonance imaging (MRI), and positron emission tomography (PET), provide useful ways to examine these alterations and to separate normal age-related changes from pathological states. Because functional disturbances precede structural changes determined by X-CT or MRI, the *in vivo* imaging obtained with PET may be abnormal, whereas the brain anatomy appears normal.

One trend is to apply target-specific PET probes for quantitative imaging of the specific neurological target molecules related to diseases, such as the dopaminergic system for schizophrenia [1] and Parkinson's disease (PD) [2], the serotonergic system for depression [3], and the cholinergic system for AD-type dementia [4]. Another trend is to measure more general indices for the pathophysiological abnormalities in diseases. To diagnose these diseases and to assess the treatment efficacy of developing drug candidates noninvasively with PET, we have anticipated PET probes that can provide general indices of brain function, such as regional cerebral blood flow (rCBF) and regional cerebral metabolic rate of oxygen ($rCMRO_2$), both of which have been recognized to be the gold standard indices for cerebral functions [5]. Other useful indicators are the regional cerebral metabolic rate of glucose (rCMRglc) assessed with ^{18}F-fluoro-2-deoxy-D-glucose (^{18}F-FDG; **Figure 1C**) [6]. PET using ^{18}F-FDG is a well-established technique for the quantitative imaging of brain function in the living brain. Some research demonstrated that ^{18}F-FDG could predict an onset of AD. However, as demonstrated in the brains of rat and monkey ischemic models [7, 8], the unexpectedly high uptake of ^{18}F-FDG in damaged areas suggested that ^{18}F-FDG was taken up into not only normal tissues but also inflammatory regions with microglial activation, which hampers the accurate diagnosis of brain function using ^{18}F-FDG.

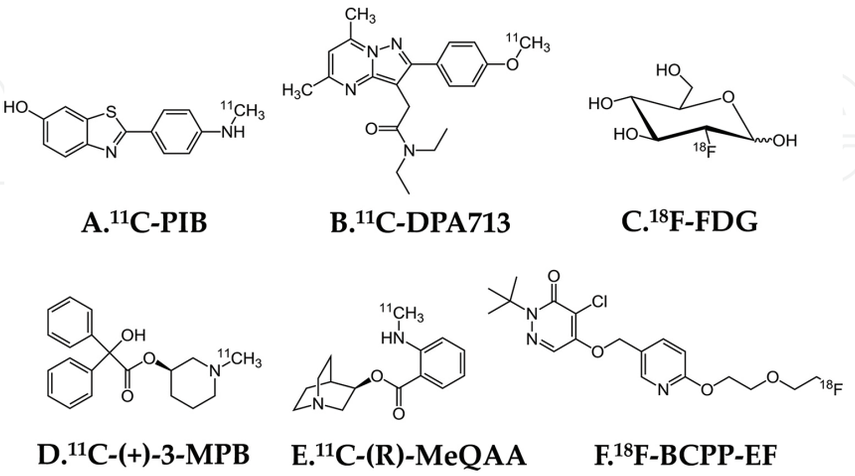

Figure 1. PET probes used: (A) ^{11}C-PIB for Aβ, (B) ^{11}C-DPA-713 for TSPO, (C) ^{18}F-FDG for rCMRglc, (D) ^{11}C-(+)-3-MPB for mAChR, (E) ^{11}C-(*R*)-MeQAA for α7-nAChR, and (F) ^{18}F-BCPP-EF for MC-I.

http://dx.doi.org/10.5772/62901

Several hypotheses of aging at the molecular level, such as shortening of telomerase, DNA methylation, reactive oxygen species (ROS) generation, and mitochondrial abnormalities, have been proposed. Among these, the "mitochondrial free radical theory of aging" has been highlighted [9]. In mammalian cells, the electron transport chain in mitochondria consists of five complexes from I to V, and the main role of mitochondria was recognized to be energy transduction of ATP. Their dysfunction was thought to be limited to ATP deficiency resulting in necrotic cell death; however, the mechanisms of cell death have been found to include mitochondrial contribution to oxidative stress and apoptosis [10]. Previous studies demonstrated an age-related increase in ROS production using rat brain homogenates [11], cortical slices [12], or synaptosomes [13]. Furthermore, mitochondrial dysfunction contributes to the pathophysiology of acute and chronic neurodegenerative disorders [14].

In the present chapter, the capability of assessment of mitochondrial complex I (MC-I) activity is introduced for detection of neurodegenerative damage associated with Aβ deposition. We recently developed and evaluated ^{18}F-2-tert-butyl-4-chloro-5-{6-[2-(2-fluoroethoxy)-ethoxy]-pyridin-3-ylmethoxy}-2H-pyridazin-3-one (^{18}F-BCPP-EF), a novel PET probe for MC-I activity (**Figure 1E**) [15]. The translational research has been conducted using an animal PET to assess the aging as well as Aβ deposition effects on MC-I activity in the living brains of young (3–5 years old, corresponding to high-teens in humans) and aged (20–24 years old, corresponding to 75 years old and more) male monkeys [16, 17].

2. Aging and cholinergic neuronal system

There have been a number of reports on age-related alterations in neurochemical and neurophysiological functions in the brain, associated with changes in the neurotransmitter synthesis in presynaptic neurons, release into synaptic cleft, reuptake availability, binding to receptors, and signal transduction, all of which are related to the declines of specific motor, cognitive and emotional functions in primates. Among the variety of neurotransmitter receptors, we focused on the effects of aging process on cholinergic receptors, which had previously assessed in the postmortem primate brain tissues [18].

2.1. Aging effects on muscarinic cholinergic receptor function

The cholinergic receptor (AChR) population is divided into muscarinic (mAChR) and nicotinic (nAChR) subclasses in the central nervous system (CNS), and the CNS mAChR system plays an important role in memory and cognitive functions. AD is neuropathologically characterized by the presence of neurofibrillary tangles with the deposition of Hyperphosphorylated tau protein inside nerve cells and senile plaques with extracellular aggregation of Aβ protein [19, 20]. Accompanied with tau and Aβ depositions, loss of cholinergic neurons in the forebrain, reduced cholinergic activity in the hippocampus and cortical loss of choline acetyltransferase, and reduced central mAChR binding have been observed in the brain of AD patients [21]. The severity of these cholinergic abnormalities is closely correlated with the degree of memory impairment in aged monkeys [22] and dementia patients [21].

Several antagonist-based ^{11}C-labeled PET probes for imaging mAChR have been developed and attempted to determine quantitatively the age-related alterations of mAChR in the living brain using ^{11}C-benztropine [23], *N*-^{11}C-methyl-4-piperidyl benzilate (^{11}C-4-MPB) [24], and ^{11}C-tropanyl benzilate (TBZ) [25]. These PET probes for mAChR, however, showed relatively low uptake to the brain and also slow dissociation rates from mAChR, which may limit the estimation of the density of binding sites *in vivo* [26]. To solve these problems, we proposed a novel mAChR probe, *N*-^{11}C-methyl-3-piperidyl benzilate (^{11}C-3-MPB) (**Figure 1D**) [27, 28], and assessed the aging effects on mAChR binding in comparison to young and aged monkeys [29].

^{11}C-(+)3-MPB was labeled by *N*-methylation of respective nor-compound with ^{11}C-methyl iodide converted from ^{11}C-CO_2 by $LiAlH_4$ reduction followed by reaction with HI [27, 28]. A monkey (*Macaca mulatta*) was seated on a monkey chair under conscious condition and fixed with stereotactic coordinates under conscious state [30]. For the kinetic analysis of ^{11}C-(+)3-MPB binding, arterial blood sampling was conducted to determine the input function using metabolic profile in plasma. The PET data obtained were reconstructed by the filtered back-projection (FBP) method. Volumes of interest (VOIs) in brain regions were drawn manually on the MRI, and VOIs of MRI were superimposed on the coregistered PET images to measure the time activity curves (TACs) of each PET probe for kinetic analyses using Logan graphical analysis with metabolite-corrected plasma input in the living brain [31].

The TACs of ^{11}C-(+)3-MPB in the frontal, temporal, and occipital cortices reached their peaks 40 min after injection, whereas the striatal and hippocampal regions reached peak values 60

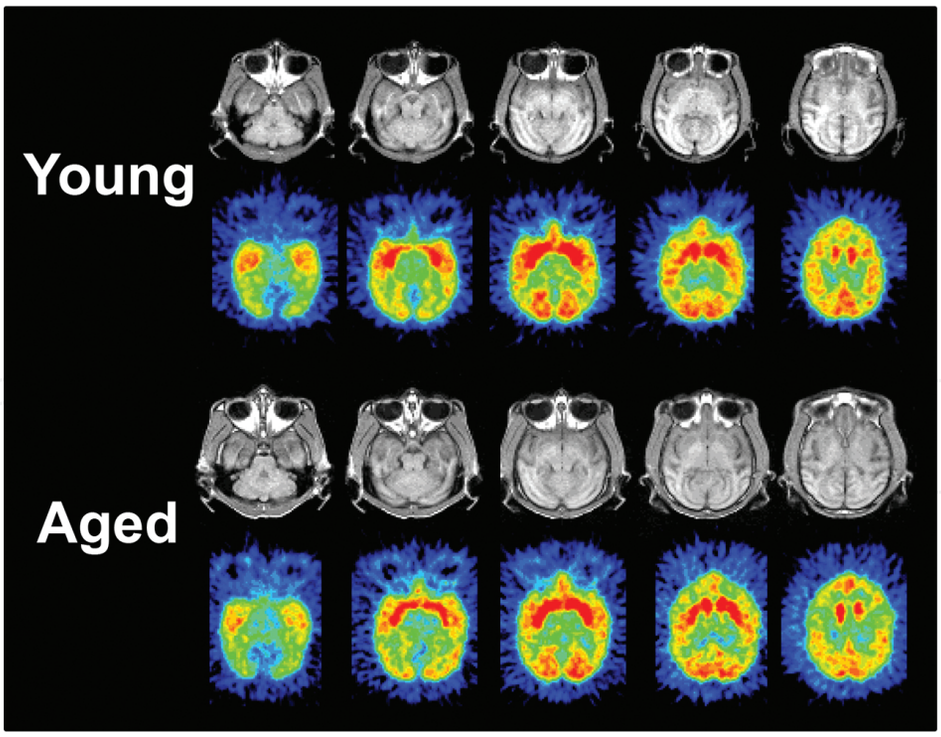

Figure 2. MRI and PET images of ^{11}C-(+)3-MPB in the young and aged monkey brains (*M. mulatta*). PET data were collected in the conscious state with a high-resolution PET scanner. Each PET image was generated by summation of image data from 60 to 91 min post-injection. The stereotactic coordinates of PET and MRI were adjusted based on the orbitomeatal (OM) line.

http://dx.doi.org/10.5772/62901

min after injection [28]. In aged monkeys, the TACs of ^{11}C-(+)3-MPB in regions rich in mAChR peaked at earlier time points, with faster elimination rates than those in young monkeys. As a result of Logan graphical analysis using metabolite-corrected plasma input, significant age-related alterations of the *in vivo* binding of ^{11}C-(+)3-MPB were observed in the temporal and frontal cortices and the striatum (**Figure 2**). Aged animals showed the age-related reduction of the maximum number of binding sites (B_{max}) of mAChR, whereas there were no age-related alterations of the affinity (1/Kd) of mAChR [29].

2.2. Aging effects on nicotinic cholinergic receptor function

The CNS AChR systems, classified into mAChR and nAChR, play an important role in memory and cognitive functions. In the last two decades, 17 different nAChR subunits (α1–α10, β1–β4,γ, δ and ε) have been cloned, and the prominent nAChRs are the α4β2 heteromeric and α7 homomeric subtypes in the brain [32]. Among them, because α7 has high permeability for Ca^{2+}, it can be assumed that, in addition to the ionotropic function induced by membrane depolarization, α7-nAChR is associated with metabotropic activity coupled to Ca^{2+}-regulated second-messenger signaling required for the modulation of neuron excitability, neurotransmitter release, induction of long-term potentiation (LTP), and cognitive-associated processing of learning and memory. In addition, α7-nAChR may contribute to neuroprotection by modulating the neurotrophic system crucial for the maintenance of cholinergic neuron integrity and also by stimulating signal transduction pathways that support neuron survival [32].

A PET study indicated that decreases in ^{11}C-nicotine brain uptake were significantly correlated with cognitive deficits in AD patients [33]; however, nAChR deficits in the different types of dementia are assumed to be reflected by subtype and region specificity. For the noninvasive imaging of α7-nAChR with more subtype specificity, several ^{11}C-labeled PET probes have been developed and evaluated, including ^{11}C-CHIBA-1001, ^{11}C-A-582941, and ^{11}C-A-844606 [34]. However, because of low brain uptake, high nonspecific binding, and/or low selectivity to α7-nAChR against 5-HT_3R, almost none of these PET probes have demonstrated clinically useful specific binding to α7-nAChR in nonhuman primate brain. Because we recently developed novel PET probes for α7-nAChR, (*R*)-2-[^{11}C]methylamino-benzoic acid 1-azabicycle[2.2.2]oct-3-yl ester [^{11}C-(*R*)-MeQAA; **Figure 1E**] [35], the aging effects on α7-nAChR binding was assessed using ^{11}C-(*R*)-MeQAA in comparison to young and aged monkeys [36].

^{11}C-(*R*)-MeQAA was labeled by *N*-methylation of respective nor-compounds [(*R*)-BH_3QAA] with ^{11}C-methyl triflate prepared from ^{11}C-methyl iodide through a glass column containing silver triflate [35]. PET measurements of conscious monkeys were conducted as described in Section 2.2 with arterial blood sampling for plasma metabolic analysis followed by PET image reconstruction and TAC acquisition in the VOIs for kinetic analyses. The values of nondisplaceable binding potential (BP_{ND}) were evaluated by two-compartment models (2-TC) analysis using the metabolite-corrected plasma input [37] and simplified reference tissue model (SRTM) analysis using the TAC in the cerebellum as an indirect input function [38].

^{11}C-(*R*)-MeQAA images in the brain of young normal monkeys, showing high and heterogeneous uptake of [^{11}C](*R*)-MeQAA into the brain, were determined between 60 and 90 min after the bolus injection. The uptake of radioactivity was high in the thalamus and striatum,

intermediate in the hippocampus, frontal, temporal, and occipital cortices, and low in the cerebellum [35, 36]. The uptake of ^{11}C-(*R*)-MeQAA was significantly higher than that of ^{11}C-(*S*)-MeQAA in the thalamus, hippocampus, and cortical regions, and the specific binding of ^{11}C-(*R*)-MeQAA was inhibited by the preadministration of SSR180711, an α7-nAChR partial agonist [35]. In contrast, the uptake of ^{11}C-(*R*)-MeQAA into the cerebellum of monkeys was not affected by SSR180711 [35], suggesting that the cerebellum could be applicable for the reference region for the quantitative analysis of ^{11}C-(*R*)-MeQAA binding in the living brain. The clearance rate of ^{11}C-(*R*)-MeQAA in plasma was rapid and relatively stable in plasma. To determine the practicality of the simplified analytical method of ^{11}C-(*R*)-MeQAA with SRTM to calculate the BP_{ND} using the TAC in the cerebellum as an indirect input function, we verified it by correlation analyses with 2-TC-BP_{ND} values calculated using the metabolite-corrected plasma input. Because of a good correlation between 2-TC and SRTM analyses, ^{11}C-(*R*)-MeQAA binding to α7-nAChR in young and aged monkey brain was determined as the SRTM-BP_{ND} values without arterial blood sampling to avoid excessive stress on aged animals. When determining the aging effects on ^{11}C-(*R*)-MeQAA binding, all regions, except the occipital cortex, revealed no significant differences in the BP_{ND} values of ^{11}C-(*R*)-MeQAA in the brains of aged and young animals [36]. Although human aging is known to preferentially affect the rCMRglc in the frontal and temporal lobes, our previous studies reported that the occipital cortex showed the most profound reductions of CBF [39], rCMRglc [39], and MC-I [16] in aged monkeys. Because the differences in cortical activity between monkey and human reflect the evolutionary significance of their frontal cortex, the most marked age-related alterations of α7-nAChR activity would be determined in regions such as the frontal cortex, not in the occipital cortex, in humans. These results apparently revealed that aging effects were much less on α7-nAChR compared to mAChR in the living brain.

3. Aging and MC-I activity

Mitochondria are called ”cellular power plants“ because they generate most of the ATP used as a source of chemical energy. In mammalian cells, the electron transport chain in mitochondria consists of five complexes from I to V, and complex I (MC-I; NADH-ubiquinone oxidoreductase, EC 1.6.5.3) is the first and rate-limiting step of the overall respiratory activity and oxidative phosphorylation under physiological conditions. Glucose is converted to pyruvate followed by transformation into acetyl-CoA by pyruvate dehydrogenase (PDH) in the mitochondria, which is subsequently fed into the tricarboxylic acid (TCA) cycle, ultimately producing ATP via the electron transport system and oxidative phosphorylation (which is indispensable for cell survival). Mitochondrial dysfunction contributes to the pathophysiology of neurodegenerative diseases [40], some part of which has been considered to relate to the fact that mitochondria are the main intracellular source of ROS in cells and also the main target of ROS-mediated damage. Noninvasive assessment of living brain could be useful for the diagnostic, prognostic, and treatment monitoring of neurodegenerative diseases related to impaired MC-I function; however, no proper PET probes for MC-I imaging in the brain have been developed prior to those that we have recently described [15].

http://dx.doi.org/10.5772/62901

3.1. Development of PET probe for MC-I imaging

As PET probe for MC-I imaging, BMS-747158-01 showed inhibitory activity on MC-I function by binding to MC-I, and its F-18 derivative ^{18}F-BMS-747158-01 was originally developed as a myocardial perfusion imaging agent [41]. However, we also realized that ^{18}F-BMS-747158-01 revealed relatively high nonspecific binding in the brain based on the lower degree of inhibition with rotenone, a specific MC-I inhibitor, in both *in vitro* and *in vivo* assessments [7, 8]. To solve the problem, we redesigned to modify the chemical structure of ^{18}F-BMS-747158-01 to induce lower lipophilicity and lower affinity [15, 42]. We recently developed a novel PET probe, ^{18}F-BCPP-EF, and evaluated its properties in the *in vitro* and *in vivo* assessments [7, 8, 15, 16].

For the analysis of the affinity of ^{18}F-BCPP-EF, an *in vitro* binding assay was conducted using ^{3}H-dihydrorotenone and bovine cardiomyocyte submitochondrial particles (SMP) to determine the 50% inhibition (IC_{50}) values, which were converted to the inhibition constant (Ki). ^{18}F-BCPP-EF was radiolabeled by the nucleophilic ^{18}F-fluorination of the corresponding tosylate precursor, toluene-4-sulfonic acid 2-{2-[5-(1-tert-butyl-5-chloro-6-oxo-1,6-dihydro-pyridazin-4-yloxymethyl)-pyridin-2-yloxy]-ethoxy}-ethyl ester [15]. For the assessment of binding specificity of the PET probe to MC-I, vehicle or rotenone, a specific MC-I inhibitor, at a dose of 0.1 mg/kg was infused to anesthetised rats or conscious monkeys through a vein for 1 h, and then ^{18}F-BCPP-EF was injected as a bolus for PET measurement. PET measurements of young monkeys (3–5 years old) were conducted under conscious state as described in Section 2.2 with arterial blood sampling for plasma metabolic analysis followed by PET image reconstruction and TAC acquisition in the VOIs aided by MRI of individual animals for kinetic analyses [16, 17]. The total distribution volume (DV) values were evaluated by Logan plot graphical analysis using the metabolite-corrected plasma input [33].

^{18}F-BCPP-EF showed the lower affinity (Ki=2.31 nM) with lower lipophilicity ($logD_{7.4}$=3.03) for MC-I of bovine cardiomyocytes than that of BMS-747158-01 (Ki=0.95 nM, $logD_{7.4}$=3.69). In PET study in rats, the radioactivity level of ^{18}F-BCPP-EF in the brain showed rapid uptake and gradual decrease with time just after the injection under vehicle condition. In the heart, ^{18}F-BCPP-EF exhibited slow accumulation up to 30 min after the injection followed by a slight washout. With preadministration of rotenone, although a dose escalation study of rotenone was impossible because of its lethal effects on cardiac function, a significant reduction of ^{18}F-BCPP-EF uptake was observed in the brain and heart, even at a relatively low dose of 0.1 mg/kg/h. ^{18}F-BMS-747158-01 showed a tendency of decreased brain uptake with rotenone infusion but was not fully inhibited [7].

In the conscious monkey brain, TACs of ^{18}F-BCPP-EF peaked between 10 and 20 min after the injection, except in the occipital cortex (40 min), followed by the gradual elimination with time. With preadministration of rotenone, a specific MC-I inhibitor, at a dose of 0.1 mg/kg/h, the uptake of ^{18}F-BCPP-EF into the brain, especially in the frontal and temporal cortices and striatum, was significantly facilitated just after the injection followed by faster elimination than normal from the brain regions. The washout and metabolic rates of ^{18}F-BCPP-EF in plasma were rapid; only 10% of nonmetabolized ^{18}F-BCPP-EF was detected 60 min after the injection, which was were nearly identical with that of rotenone-treated animals. The DV values

calculated by Logan plot graphical analysis were the highest in the occipital cortex, higher in the striatum, intermediate in the frontal and temporal cortices and cerebellum, and lowest in the hippocampus of young monkey. Rotenone administration resulted in a significant and marked reduction of the binding of ^{18}F-BCPP-EF to MC-I in the living monkey brain [16]. Taken together, these results clearly suggested that ^{18}F-BCPP-EF was a useful PET probe for the quantitative imaging of MC-I activity in the living brain.

3.2. Aging effects on MC-I activity

Several hypotheses of aging have been proposed, and mitochondrial respiratory chain failures have been implicated as factors in the aging process, which was called the "mitochondrial free radical theory of aging" [9–13]. This theory is based on the results that (1) mitochondrial ROS production increases with age, (2) the activity of ROS-scavenging enzymes declines with age, (3) mutations of mitochondrial DNA (mtDNA) accumulate during aging, and (4) somatic mtDNA mutations impair respiratory chain function, which results in a further increase in ROS production [9–13]. Mitochondria are the main intracellular source of ROS and also the main target of oxyradical-mediated damage, and cumulative free radical damage leads to significant changes in brain mitochondrial function.

As described in Section 3.1, because we could confirm the capability of ^{18}F-BCPP-EF as PET probe for the noninvasive assessment of MC-I activity in the living brain, we further explored to see the aging effects on MC-I activity in comparison to young and aged monkeys under conscious condition [16]. All study procedures were identical as described in Section 3.1, except that the subjects were aged male monkeys (20–24 years old).

Aided by MRI of individual monkeys, the VOIs were set on PET images of ^{18}F-BCPP-EF to obtain TACs. The peak of ^{18}F-BCPP-EF slightly shifted to a later time period between 20 and 30 min after the injection and also provided significantly lower levels than those in young animals shown in Section 3.1. The washout and metabolic patterns of ^{18}F-BCPP-EF in plasma of aged monkeys were nearly identical to those in young animals. When determining the effects of aging on ^{18}F-BCPP-EF binding to MC-I assessed by Logan plot graphical analysis, the data revealed significantly lower DV values of ^{18}F-BCPP-EF in every brain region analyzed in aged animals compared to those in young ones [16].

The remarkable finding of the present study was that ^{18}F-BCPP-EF detected the age-related reduction of MC-I activity in the living brain of monkey under conscious conditions with PET (**Figure 3**). It was of interest that the activity of complexes I and IV decreased with age in the brain of humans [43], whereas that of complexes II, III, and V remained mostly unchanged [44]. Because all these findings described above were obtained by the *in vitro* assessments of dissected organ samples, the present data are the first to demonstrate the alterations of MC-I activity in the living brain of a nonhuman primate by a noninvasive method using ^{18}F-BCPP-EF and PET [16].

http://dx.doi.org/10.5772/62901

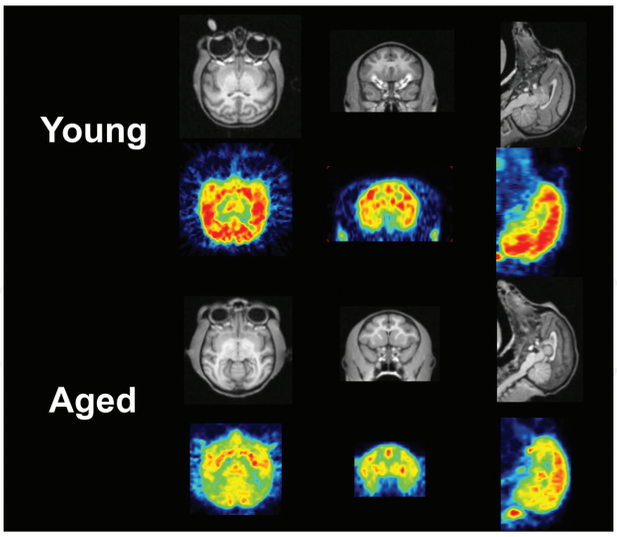

Figure 3. MRI and PET images of ^{18}F-BCPP-EF in young and aged monkeys (*M. mulatta*). PET scans were acquired for 91 min after ^{18}F-BCPP-EF injection with sequential arterial blood sampling. The binding of ^{18}F-BCPP-EF to MC-I was calculated using Logan graphical analysis with metabolite-corrected plasma input.

4. Effects of Aβ deposition on AChR and MC-I

Hallmark pathologies of AD have been assumed to the formation of extracellular aggregation of Aβ protein (senile plaques) [19] and intraneuronal aggregation of phosphorylated tau protein (neurofibrillary tangle) [20], pathogenic microglial activation [45], and oxidative stress reactions [13]. Furthermore, recent reports suggested that nondeposited and nonfibrillar assemblies of Aβ peptides are considered to play a primary role in AD, which might be precursors in fibrillogenesis to mediate the neurotoxicity, including oxidative stress in AD [46]. This session discusses the effects of Aβ-related pathological changes on nAChR binding [36] and also on MC-I activity [17] assessed in aged monkey brain using animal PET.

4.1. Aging effects on Aβ deposition and neuroinflammation

For the quantitative measurements of Aβ deposition in the living brain, ^{11}C-PIB was synthesized by *N*-methylation of nor-compound *N*-desmethyl-PIB with ^{11}C-methyl triflate (**Figure 1A**) [47]. For the assessment of neuroinflammation, ^{11}C-DPA-713 was synthesized by *N*-methylation of nor-compound *N*-desmethyl-DPA with ^{11}C-methyl triflate (**Figure 1B**) [48]. PET measurements with these two PET probes were conducted under conscious state as described in Section 2.2. For the analysis of ^{11}C-PIB uptake, standard uptake value (SUV) images were created, and the VOIs were set on each SUV images with the aid of MRI. For the analysis of ^{11}C-DPA-713 uptake, SUV images were created, and VOIs were set on each SUV images.

We had previously found that some, but not all, of aged monkeys exhibited higher ^{11}C-PIB uptake than young ones, suggesting Aβ deposition even in the brain of monkey [49]. Although the SUVs of ^{11}C-PIB were slightly high in the striatal regions, hippocampus, parietal cortex,

and thalamus in aged monkeys, it was reported that aged monkeys did not reveal as high Aβ deposition as determined in AD patients [50] and also that no species besides humans has yet shown drastic neuron loss or cognitive decline approaching clinical-grade AD in humans. The SUVs of ^{11}C-DPA-713 were relatively high in the striatal regions, hippocampus, temporal cortex, and thalamus. The plot of SUV of ^{11}C-DPA-713 against SUV of ^{11}C-PIB revealed significant positive correlation both in the cortical regions. When rCMRglc ratio is plotted against SUV of ^{11}C-DPA-713, the results provided the significant positive correlation in the cortical regions. There results strongly suggest that the Aβ deposition as measured with ^{11}C-PIB induced neuroinflammation with microglial activation as determined with ^{11}C-DPA-713 as well as ^{18}F-FDG (**Figure 4**).

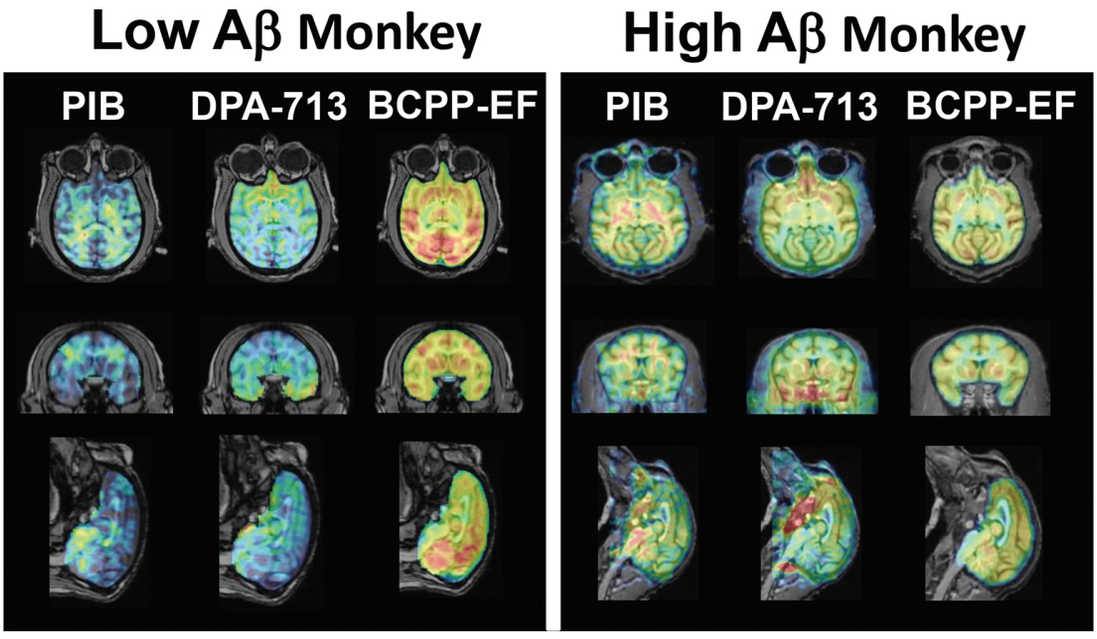

Figure 4. PET/MRI fusion images of ^{11}C-PIB, ^{11}C-DPA-713, and ^{18}F-BCPP-EF uptake in the brains of aged monkeys (*M. mulatta*). ^{18}F-BCPP-EF brain imaging was performed in monkey 1 with the highest binding of all 20 animals in the conscious state and in monkey 2 with the lowest binding.

4.2. Effects of Aβ deposition on nAChR binding

Postmortem studies of human brains have suggested that a deficit of α7-nAChR is related to AD, dementia with Lewy bodies, and schizophrenia [32]. Aβ has a high affinity to α7-nAChR upon being enriched in basal forebrain areas, and initial Aβ deposition in early AD overlaps with α7-nAChR expression in these regions [51]. α7-nAChR facilitates binding, internalization, and accumulation of $A\beta_{1–42}$ and may result in the selective vulnerability of specific cells expressing α7-nAChR [52]. Oligomers of Aβ disrupt synaptic plasticity and cognitive function when administered at nanomolar range concentration through the modulation of NMDA receptor function to depress NMDA-evoked currents [53, 54].

To assess the effect of Aβ deposition on α7-nAChR function, the correlation between ^{11}C-PIB uptake and ^{11}C-(*R*)-MeQAA was analyzed [36]. As described in Section 2.2, all regions, except

http://dx.doi.org/10.5772/62901

the occipital cortex, revealed no significant differences in the BP_{ND} values of ^{11}C-(*R*)-MeQAA in the brains of aged and young animals. However, of interest, when the BP_{ND} values of ^{11}C-(*R*)-MeQAA are plotted against the SUVR of ^{11}C-PIB in the corresponding VOIs of aged animals, the results indicated a significant positive correlation between them (**Figure 5**). The α7-nAChR had been assumed to decrease with the aging process; however, the data seem to be controversial because of the dose-dependent interaction aspects between of Aβ and α7-nAChR. In young and normal conditions, there is an equilibrium between production and elimination of Aβ, which maintains Aβ in a steady state to perform physiologic roles by the interaction with α7-nAChR; thus, low (on the order of picomolar) concentrations of $Aβ_{1–42}$ may play a role in modulating synaptic plasticity and enhancing cognitive function in mice via interaction with α7-nAChR, probably in presynaptic neurons [55]. In aging with pathologic conditions, the balance between Aβ formation and clearance is impaired, which leads to Aβ accumulation and α7-nAChR deficit as observed in postmortem brains of AD patients [32]. These results suggest that α7-nAChR-Aβ interaction has dual effects on brain function following aging or injury as well as preserving physiologic roles, causing the controversial results in the aging effects on the α7-nAChR level. One previous study clearly demonstrated the significant reduction of α7-nAChR level in neurons and also Aβ-induced up-regulation of α7-nAChR on astrocytes in postmortem AD brain compared to that in age-matched control [56]. α7-nAChR may be chronically inactivated in an antagonistic fashion through prolonged interaction with increased levels (on the order of nanomolar) of Aβ, resulting in the up-regulation of α7-nAChR.

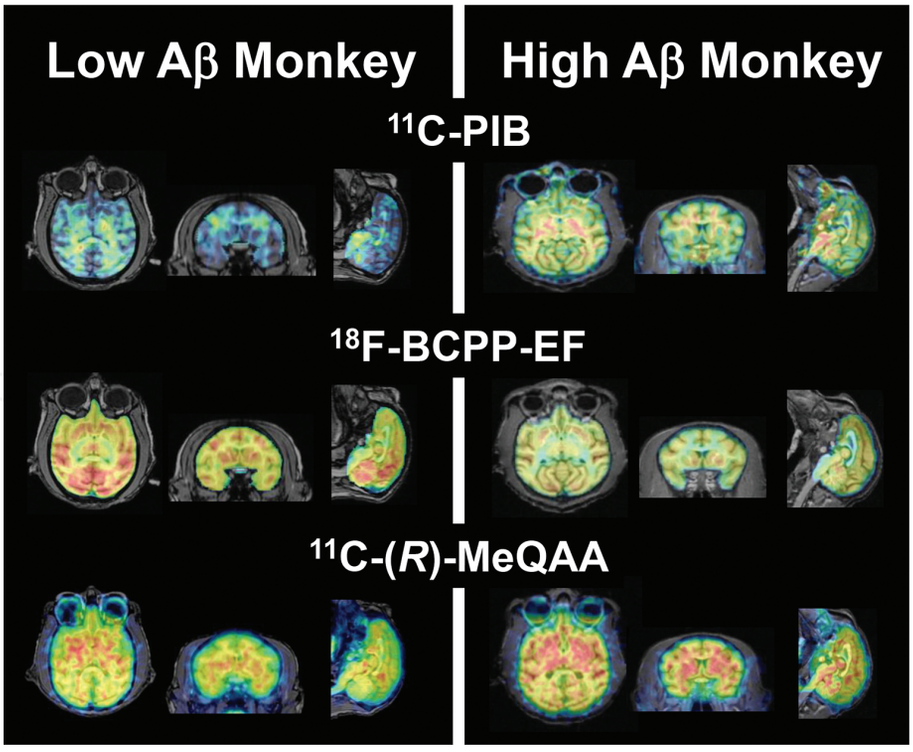

Figure 5. PET/MRI fusion images of ^{11}C-PIB, ^{18}F-BCPP-EF, and ^{11}C-(*R*)-MeQAA in the brains of aged monkeys (*M. mulatta*). PET images of an aged monkey with the lowest and highest ^{11}C-PIB uptake are shown along with ^{18}F-BCPP-EF and ^{11}C-(*R*)-MeQAA.

4.3. Effects of Aβ deposition on MC-I activity

As shown in Section 3.2, ^{18}F-BCPP-EF binding to MC-I in each brain region indicated much larger variation (CV=25.1%) in aged animals than in young ones (7.4%) [16]. Since we had previously found that some of the aged monkeys exhibited high ^{11}C-PIB uptake, suggesting Aβ deposition in the brain [49], the effects of Aβ deposition level assessed in Section 4.1 on MC-I activity evaluated in Section 3.2 were determined. When the ^{18}F-BCPP-EF binding is plotted against the ^{11}C-PIB uptake in the corresponding VOIs of all animals, the results indicated a significant reversal correlation (**Figure 4**). In contrast, no significant relationships were observed in the plot of rCMRglc measured using ^{18}F-FDG against ^{11}C-PIB uptake in the cerebral cortical regions [17]. There results strongly suggest that the Aβ deposition as measured with ^{11}C-PIB induced neuroinflammation with microglial activation as determined with ^{11}C-DPA-713 as well as ^{18}F-FDG. Apart from developed cells such as neurons, activated inflammatory cells produce lactate from glucose, known as the Warburg effect [57] or aerobic glycolysis, accounting for only approximately 5% glucose utilization in oxidative phosphorylation. Because activated inflammatory cells exclusively produce ATP through enhanced glycolysis with a low contribution of the electron transport system, these cells need more glucose to survive than normal neuronal and glial tissues, resulting in the higher ^{18}F-FDG uptake in the neurodegenerative damaged regions. The present results demonstrated that ^{18}F-BCPP-EF could be used to image MC-I activity specifically as well as to detect impaired MC-I activity correlated to Aβ deposition in the living brain of monkeys.

5. Conclusions

In this chapter, the effects of Aβ deposition on α7-nAChR binding, TSPO activity, an established marker of microglial activation, and rCMRglc were assessed simultaneously with MC-I activity. PET using ^{18}F-FDG is a well-established technique for the quantitative imaging of brain function as rCMRglc in the living brain. However, the unexpectedly high uptake of ^{18}F-FDG in damaged brain regions suggested that ^{18}F-FDG was taken up into not only normal tissues but also inflammatory regions with microglial activation, which hampers the accurate diagnosis of brain function using ^{18}F-FDG. Neuroinflammation has recently emerged in several neurodegenerative diseases, including schizophrenia, depression, autism, PD, and AD. PET measurements of MC-I activity using ^{18}F-BCPP-EF will be a superior diagnostic, prognostic, and treatment monitoring tool for AD-type dementia without being affected by inflammation.

Author details

Hideo Tsukada*

Address all correspondence to: tsukada@crl.hpk.co.jp

Central Research Laboratory, Hamamatsu Photonics K.K., Hamamatsu, Japan

References

[1] Patel NH, Vyas NS, Puri BK, Nijran KS, Al-Nahhas A. Positron emission tomography in schizophrenia: A new perspective. J Nucl Med. 2010;51:511–520. DOI: 10.2967/jnumed.109.066076.

[2] Brooke DJ. Imaging approaches to Parkinson disease. J Nucl Med. 2010;51:596–609. DOI: 10.2967/jnumed.108.059998.

[3] Neyer JH. Neuroimaging markers of cellular function in major depressive disorder: Implications for therapeutics, personalized medicine, and prevention. Clin Pharmacol Ther. 2012;91:201–214. DOI: 10.1038/clpt.2011.285.

[4] Kadir A, Nordberg A. Target-specific PET probes for neurodegenerative disorders related to dementia. J Nucl Med. 2010;51:1418–1430. DOI: 10.2967/jnumed.110.077164.

[5] Lammertsma AA, Heather JD, Jones T, Frackowiak RSJ, Lenzi GL. A statistical study of the steady-state technique for measuring regional cerebral blood flow and oxygen utilization using ^{15}0. J Comput Assist Tomogr. 1982;6:566–573.

[6] Phelps ME, Huang SC, Hoffman El, Selin CS, Sokoloff L, Kuhl DE. Tomographic measurement of local cerebral glucose metabolic rate in humans with (F-18) 2-fluoro-2-deoxyglucose: Validation of method. Ann Neurol. 1979;6:371–388. DOI: 10.1002/ana.410060502.

[7] Tsukada H, Nishiyama S, Fukumoto D, Kanazawa M, Harada N. Novel PET probes ^{18}F-BCPP-EF and ^{18}F-BCPP-BF for mitochondrial complex I: A PET study in comparison with ^{18}F-BMS-747158-02 in rat brain. J Nucl Med. 2014;55:473–480. DOI: 10.2967/jnumed.113.125328.

[8] Tsukada H, Ohba H, Nishiyama S, Kanazawa M, Kakiuchi T, Harada N. PET imaging of ischemia-induced impairment of mitochondrial complex I function in monkey brain. J Cereb Blood Flow Metab. 2014;34:708–714. DOI: 10.1038/jcbfm.2014.5.

[9] Bratic A, Larsson NG. The role of mitochondria in aging. J Clin Invest. 2013;123:952–957. DOI: 10.1172/JCI64125.

[10] Ankarcrona M, Dypbukt JM, Bonfoco E, Zhivotovsky B, Orrenius S, Lipton SA, Nicotera P. Glutamate-induced neuronal death: A succession of necrosis or apoptosis depending on mitochondrial function. Neuron. 1995;15:961–973. DOI: 10.1016/0896-6273(95)90186-8.

[11] Baek BS, Kwon HJ, Lee KH, Yoo MA, Kim KW, Ikeno Y, Yu BP, Chung HY. Regional difference of ROS generation, lipid peroxidation, and antioxidant enzyme activity in

rat brain and their dietary modulation. Arch Pharm Res. 1999;22:361–366. DOI: 10.1007/BF02979058.

[12] Kannurpatti SS, Sanganahalli BG, Mishra S, Joshi PG, Joshi NB. Glutamate-induced differential mitochondrial response in young and adult rats. Neurochem Int. 2004;44:361–369. DOI: 10.1007/BF02979058.

[13] Choi BH. Oxidative stress and Alzheimer's disease. Neurobiol Aging. 1995;16:675–678. DOI: 10.1016/0197-4580(95)00065-M.

[14] Schon EA, Przedborski S. Mitochondria: The next (neurode)generation. Neuron. 2011;70:1033–1053. DOI: 10.1016/j.neuron.2011.06.003.

[15] Harada N, Nishiyama S, Kanazawa M, Tsukada H. Development of novel PET probes, [^{18}F]BCPP-EF, [^{18}F]BCPP-BF, and [^{11}C]BCPP-EM for mitochondrial complex I imaging. J Labelled Compd Radiopharm. 2013;56:553–561. DOI: 10.1002/jlcr.3056.

[16] Tsukada H, Ohba H, Kanazawa M, Kakiuchi T, Harada N. Evaluation of ^{18}F-BCPP-EF for mitochondrial complex 1 imaging in conscious monkey brain using PET. Eur J Nucl Med Mol Imaging. 2014;41:755–763. DOI: 10.1007/s00259-014-2821-8.

[17] Tsukada H, Nishiyama S, Ohba H, Kanazawa M, Kakiuchi T, Harada N. Comparing amyloid-β deposition, neuroinflammation, glucose metabolism, and mitochondrial complex I activity in brain: A PET study in aged monkeys. Eur J Nucl Med Mol Imaging. 2014;41:2127–2136. DOI: 10.1007/s00259-013-2628-z.

[18] Court JA, Lloyd S, Johnson M, Griffiths M, Birdsall NJM, Piggott MA, Oakley AE, Ince PG, Perry EK, Perry RH. Nicotinic and muscarinic cholinergic receptor binding in the human hippocampal formation during development and aging. Dev Brain Res. 1997;101:93–105. DOI: 10.1016/S0165-3806(97)00052-7.

[19] Hardy J, Selkoe DJ. The amyloid hypothesis of Alzheimer's disease: Progress and problems on the road to therapeutics. Science. 2002;297:353–356. DOI: 10.1126/science.1072994.

[20] Grundke-Iqbal I, Iqbal K, Tung YC, Quinlan M, Wisniewski HM, Binder LI. Abnormal phosphorylation of the microtubule-associated protein tau (τ) in Alzheimer cytoskeletal pathology. Proc Natl Acad Sci U S A. 1986;83:4913–4917.

[21] Terry AV Jr, Buccafusco JJ. The cholinergic hypothesis of age and Alzheimer's disease-related cognitive deficits: Recent challenges and their implications for novel drug development. J Pharmacol Exp Ther. 2003;306:821–827. DOI: 10.1124/jpet.102.041616.

[22] Tsukada H, Nishiyama S, Fukumoto D, Ohba H, Sato K, Kakiuchi T. Effects of acute acetylcholinesterase inhibition on the cerebral cholinergic neuronal system and cognitive function: Functional imaging of the conscious monkey brain using animal PET in combination with microdialysis. Synapse. 2004;52:1–10. DOI: 10.1002/syn.10310.

[23] Dewey SL, Volkow ND, Logan J, MacGregor RR, Fowler JS, Schlyer DJ, Bendriem B. Age-related decrease in muscarinic cholinergic receptor binding in the human brain

measured with positron emission tomography (PET). J Neurosci Res. 1990;27:569–575. DOI: 10.1002/jnr.490270418.

[24] Zubieta JK, Koeppe RA, Frey KA, Kilbourn MR, Mangner TJ, Foster NL, Kuhl DE. Assessment of muscarinic receptor concentrations in aging and Alzheimer disease with ^{11}C-NMPB and PET. Synapse. 2001;39:275–287. DOI: 10.1002/1098-2396(20010315)39:4<275::AID-SYN1010>3.0.CO;2–3.

[25] Lee KS, Frey KA, Koeppe RA, Buck A, Mulholland GK, David E, Kuhl DE. *In vivo* quantification of cerebral muscarinic receptors in normal human aging using positron emission tomography and [^{11}C]tropanyl benzilate. J Cereb Blood Flow Metab. 1996;16:303–310. DOI: 10.1097/00004647-199603000-00016.

[26] Koeppe RA, Frey KA, Mulholland GK. Kilbourn MR, Buck A, Lee KS, Kuhl DE. [^{11}C]Tropanyl benzilate binding to muscarinic cholinergic receptors: Methodology and kinetic modeling alterations. J Cereb Blood Flow Metab. 1994;14:85–99. DOI: 10.1038/jcbfm.1994.13.

[27] Takahashi K, Murakami M, Miura S, Iida H, Kanno I, Uemura K. Synthesis and autoradiographic localization of muscarinic cholinergic antagonist *N*-^{11}C-methyl-3-piperidyl benzilate as a potent radioligand for positron emission tomography. Appl Radiat Isot. 1999;50:521–525. DOI: 10.1016/S0969-8043(97)10155-5.

[28] Tsukada H, Takahashi K, Miura S, Nishiyama S, Kakiuchi T, Ohba H, Sato K, Hatazawa J, Okudera T. Evaluation of novel PET ligands (+)*N*-[^{11}C]methyl-3-piperidyl benzilate ([^{11}C](+)3-MPB) and its stereoisomer [^{11}C](-)3-MPB for muscarinic cholinergic receptors in the conscious monkey brain: A PET study in comparison with [^{11}C]4-MPB. Synapse. 2001;39:182–192. DOI: 10.1002/1098-2396(200102)39:2<182::AID-SYN10>3.0.CO;2-Q.

[29] Tsukada H, Kakiuchi T, Nishiyama S, Ohba H, Sato K, Harada N, Takahashi K. Age differences in muscarinic cholinergic receptors assayed with (+)*N*-[^{11}C]methyl-3-piperidyl benzilate in the brains of conscious monkeys. Synapse. 2001;41:248–257. DOI: 10.1002/syn.1082.

[30] Tsukada H, Harada N, Nishiyama S, Ohba H, Kakiuchi T, Sato K, Fukumoto D, Kakiuchi T. Ketamine decreased striatal [^{11}C]raclopride binding with no alterations in static dopamine concentrations in the striatal extracellular fluid in the monkey brain: Multiparametric PET studies combined with microdialysis analysis. Synapse. 2000;37:95–103. DOI: 10.1002/1098-2396(200008)37:2<95::AID-SYN3>3.0.CO;2-H.

[31] Logan J, Fowler J, Volkow N, Wolf AP, Dewey SL, Schlyer DJ, MacGregor RR, Hitzemann R, Bendriem B, Gatley SJ, David R, Christman DR. Graphical analysis of reversible radioligand binding from time-activity measurements applied to *N*-^{11}C-methyl-(-)-cocaine PET studies in human subjects. J Cereb Blood Flow Metab. 1990;10:740–747. DOI: 10.1038/jcbfm.1990.127.

[32] Albuquerque EX, Pereira EF, Alkondon M, Rogers SW. Mammalian nicotinic acetylcholine receptors: From structure to function. Physiol Rev. 2009;89:73–120. DOI: 10.1152/physrev.00015.2008.

[33] Kadir A, Almkvist O, Wall A, Långström B, Nordberg A. PET imaging of cortical ^{11}C-nicotine binding correlates with the cognitive function of attention in Alzheimer's disease. Psychopharmacology. 2006;188:509–520. DOI: 10.1007/s00213-006-0447-7.

[34] Wu J, Ishikawa M, Zhang J, Hashimoto K. Brain imaging of nicotinic receptors in Alzheimer's disease. Int J Alzheimer's Dis. 2010;2010:548913. DOI: 10.4061/2010/548913.

[35] Ogawa M, Nishiyama S, Tsukada H, Hatano K, Fuchigami T, Yamaguchi H, Matsushima Y, Ito K, Magata Y. Synthesis and evaluation of new imaging agent for central nicotinic acetylcholine receptor α7 subtype. Nucl Med Biol. 2010;37:347–355. DOI: 10.1016/j.nucmedbio.2009.11.007.

[36] Nishiyama S, Ohba H, Kanazawa M, Kakiuchi T, Tsukada H. Comparing α7 nicotinic acetylcholine receptor binding, amyloid-β deposition, and mitochondria complex-I function in living brain: A PET study in aged monkeys. Synapse. 2015;69:475–483. DOI: 10.1002/syn.21842.

[37] Mintun MA, Raichle ME, Kilbourn MR, Wooten GF, Welch MJ. A quantitative model for the *in vivo* assessment of drug binding sites with positron emission tomography. Ann Neurol. 1984;15:217–227. DOI: 10.1002/ana.410150302.

[38] Innis RB, Cunningham VJ, Delforge J, Fujita M, Gjedde A, Gunn RN, Holden J, Houle S, Huang SC, Ichise M, Iida H, Kimura Y, Koeppe RA, Knudsen GM, Knuuti J, Lammertsma AA, Laruelle M, Logan J, Maguire RP, Mintun MA, Morris ED, Parsey R, Price JC, Slifstein M, Sossi V, Suhara T, Votaw JR, Wong DF, Carson RE. Consensus nomenclature for *in vivo* imaging of reversibly binding radioligands. J Cereb Blood Flow Metab. 2007;27:1533–1539. DOI: 10.1038/sj.jcbfm.9600493.

[39] Noda A, Takamatsu H, Minoshima S, Tsukada H, Nishimura S. Determination of kinetic rate constants for 2-[^{18}F]fluoro-2-deoxy-D-glucose and partition coefficient of water in conscious macaques and alterations in aging or anesthesia examined on parametric images with an anatomic standardization technique. J Cereb Blood Flow Metab. 2003;23:1441–1447.

[40] Schild L, Huppelsberg J, Kahlert S, Keilhoff G, Reiser G. Brain mitochondria are primed by moderate Ca^{2+} rise upon hypoxia/reoxygenation for functional breakdown and morphological disintegration. J Biol Chem. 2003;278:25454–25460. DOI: 10.1074/jbc.M302743200.

[41] Yalamanchili P, Wexler E, Hayes M, Yu M, Bozek J, Kagan M, Radeke HS, Azure M, Purohit A, Casebier DS, Robinson SP. Mechanism of uptake and retention of F-18 BMS-747158-02 in cardiomyocytes: A novel PET myocardial imaging agent. J Nucl Cardiol. 2007;14:782–788. DOI: 10.1016/j.nuclcard.2007.07.009.

[42] Waterhouse RN. Determination of lipophilicity and its use as a predictor of blood-brain barrier penetration of molecular imaging agents. Mol Imaging Biol. 2003;5:376–389. DOI: 10.1016/j.mibio.2003.09.014.

[43] Ojaimi J, Masters CL, Opeskin K, McKelvie P, Byrne E. Mitochondrial respiratory chain activity in the human brain as a function of age. Mech Age Dev. 1999;111:39–47. DOI: 10.1016/S0047-6374(99)00071-8.

[44] Navarro A, Boveris A. The mitochondrial energy transduction system and the aging process. Am J Physiol Cell Physiol. 2007;292:C670–C686. DOI: 10.1152/ajpcell.00213.2006.

[45] Monson NL, Ireland SJ, Ligocki AJ, Chen D, Rounds WH, Li M, Huebinger RM, Cullum CM, Greenberg BM, Stowe AM, Rong Zhang R. Elevated CNS inflammation in patients with preclinical Alzheimer's disease. J Cereb Blood Flow Metab. 2014;34:30–33. DOI: 10.1038/jcbfm.2013.183.

[46] Swomley AM, Förster S, Keeney JT, Triplett J, Zhang Z, Sultana R, Butterfield DA. Aβ, oxidative stress in Alzheimer disease: Evidence based on proteomics studies. Biochim Biophys Acta. 2014;1842:1248–1257. DOI: 10.1016/j.bbadis.2013.09.015.

[47] Klunk WE, Engler H, Nordberg A, Wang Y, Blomqvist G, Holt DP, Bergstrom M, Savitcheva I, Huang GF, Estrada S, Ausen B, Debnath ML, Barletta J, Price JC, Sandell J, Lopresti BJ, Wall A, Koivisto P, Antoni G, Mathis CA, Langstrom B. Imaging brain amyloid in Alzheimer's disease with Pittsburgh Compound-B. Ann Neurol. 2004;55:306–319. DOI: 10.1002/ana.20009.

[48] Boutin H, Chauveau F, Thominiaux C, Gregoire MC, James ML, Trebossen R, Hantraye P, Dolle F, Tavitian B, Kassiou M. Receptor PET ligand for *in vivo* imaging of neuroinflammation. J Nucl Med. 2007;48:573–581. DOI: 10.2967/jnumed.106.036764.

[49] Noda A, Murakami M, Nishiyama S, Fukumoto D, Miyoshi S, Tsukada H, Nishimura S. Amyloid imaging in aged and young macaques with [^{11}C]PIB and [^{18}F]FDDNP. Synapse. 2008;62:472–475. DOI: 10.1002/syn.20508.

[50] Finch CE, Austad SN. Primate aging in the mammalian scheme: The puzzle of extreme variation in brain aging. Age. 2012;34:1075–1091. DOI: 10.1007/s11357-011-9355-9.

[51] Parri HR, Hernandez CM, Dineley KT. Research update: Alpha 7 nicotinic acetylcholine receptor mechanism in Alzheimer's disease. Biochem Pharmacol. 2011;82:931–942. DOI: 10.1016/j.bcp.2011.06.039.

[52] Nagele RG, D'Andrea MR, Anderson WJ, Wang HY. Intracellular accumulation of β-amyloid (1–42) in neurons is facilitated by the α7 nicotinic acetylcholine receptor in Alzheimer's disease. Neuroscience. 2002;110:199–211. DOI: 10.1016/S0306-4522(01)00460–2.

[53] Cleary JP, Walsh DM, Hofmeister JJ, Shankar GM, Kuskowski MA, Selkoe DJ, Ashe KH. Natural oligomers of the amyloid-β protein specifically disrupt cognitive function. Nat Neurosci. 2005;8:79–84. DOI: 10.1038/nn1372.

[54] Lesne S, Koh MT, Kotilinek L, Kayed R, Glabe CG, Yang A, Gallagher M, Ashe KH. A specific amyloid-β protein assembly in the brain impairs memory. Nature. 2006;440:352–357. DOI: 10.1038/nature04533.

[55] Puzzo D, Privitera L, Leznik E, Fa M, Staniszewski A, Palmeri A, Arancio O. Picomolar amyloid-β positively modulates synaptic plasticity and memory in hippocampus. J Neurosci. 2008;28:14537–14545. DOI: 10.1523/JNEUROSCI.2692-08.2008.

[56] Yu WF, Guan ZZ, Bogdanovic N, Nordberg A. High selective expression of α7 nicotinic receptors on astrocytes in the brains of patients with sporadic Alzheimer's disease and patients carrying Swedish APP 670/671 mutation: A possible association with neuritic plaques. Exp Neurol. 2005;192:215–225. DOI: 10.1016/j.expneurol.2004.12.015.

[57] Warburg O. On respiratory impairment in cancer cells. Science. 1956;124:267–272. DOI: 10.1126/science.124.3215.267.